

ILASS-Americas 23rd Annual Conference on Liquid Atomization and Spray Systems, Ventura,
CA, May 2011

Laboratory Measurements and Sensitivity Modeling of Droplet Characteristics and Implications for Superfog¹

Christian Bartolome^{1*}, Marko Princevac¹, Akula Venkatram¹, Shankar Mahalingam², David R.
Weise³, Gary Achtemeier⁴, Henry Vu and Guillermo Aguilar¹

1. Department of Mechanical Engineering, University of California, Riverside, CA

2. College of Engineering, University of Alabama – Huntsville, AL

3. PSW Research Station, USDA Forest Service, Riverside, CA

4. Southern Research Station, USDA Forest Service, Athens, GA

Abstract

Land management techniques in wildland areas include prescribed fires to promote biodiversity and reduce risk of severe wildfires. Loss of life, injuries, and millions of dollars spent on litigation associated with motor vehicle accidents have resulted from smoke-related visibility reduction from prescribed burns. In the southern US, prescribed fires in the winter season have special cases of visibility reductions to less than 3 meters known as superfog. The need to accurately characterize and model conditions that lead to superfog is of importance to land managers to be able to prevent dangerous low visibility situations when planning prescribed burns. Empirical relations developed for naturally occurring advection fogs relate visibility to the liquid water content (LWC). These relations suggest a relatively large LWC ($\sim 5 \text{ g m}^{-3}$) that is thermodynamically difficult to achieve to reach visibility less than 3 meters. It has been hypothesized that extremely hygroscopic cloud condensation nuclei from the smoldering phase of a fire can produce a large number of droplets smaller in size than in naturally occurring fog. Consequently, it is feasible to achieve superfog conditions at relatively low LWC ($\sim 2 \text{ g m}^{-3}$) superfog. Laboratory generated fogs resembling near superfog visibilities have been measured by Phase Doppler Particle Analyzer (PDPA) system to determine particle number density and size distribution. Measurements indicate that mean droplet diameter of $3 \mu\text{m}$ was larger than expected for superfog while producing similar low visibility conditions. A sensitivity study of droplet size distributions and number densities was carried out to understand the impact on visibility and LWC. Assuming a log normal particle size distribution, droplets of mean diameter of $2 \mu\text{m}$ or less is required low LWC to form superfog. Large standard deviations in droplet size distribution lead to conditions requiring large amounts of LWC, which are possible in the atmosphere only under extreme conditions, for significant visibility reduction. The presence of cloud condensation nuclei (CCN) from smoke has a significant impact on the droplet size distribution. Concentrations of solute CCN to form superfog was modeled, and found that for high concentrations of solute pollutants, water vapor will readily condense to a large number of droplets to form superfog. Modeling results of droplet size distribution impact on visibility is presented together with laboratory measurements of size distribution and number density during superfog generation.

*Christian Bartolome: cbartolo@engr.ucr.edu

³ This manuscript was prepared, in part, by U.S. Government employees on official time, is not subject to copyright and is in the public domain. The use of tradenames is provided for informational purposes only and does not constitute endorsement by the U.S. Department of Agriculture.

Introduction

Prescribed burns are a common tool used by wildland managers to reduce hazardous fuel accumulations, enhance wildlife habitat, and stimulate plant regeneration in the United States. Prescribed burns can also impact air quality and visibility due to the smoke and fog formation. In rare cases the smoke and fog combination has crossed over major roadways leading to visibilities less than 3 meters, a condition known as superfog (Achteimeier, 2008). Numerous tragic highway accidents such as the I-4 disaster in Florida (on January 9, 2008) have resulted from these superfog events.

Superfog is currently hypothesized to form during the smoldering phase of a wildland fire in the night hours. The smoldering phase releases primarily water vapor and particles that can act as cloud condensation nuclei (CCN). Mixing between the cool ambient air, hot water vapor, and CCN will lead to condensation into droplets. The presence of numerous droplets in air causes extreme light scattering, thereby reducing visibility. Visibility is strongly dependent on the size distribution of particles and number concentration of droplets.

In this paper, we report on the results from laboratory scale experiments and modeling to determine the range of conditions favorable for superfog formation and thereby improve our understanding of the phenomenon. Additional theoretical development that expands on the initial framework developed by Achteimeier 2008 work is presented.

Theoretical Background

Visibility reduction by water droplets

The core variables for the characterization of superfog are liquid water content, extinction coefficient, and visibility. Liquid water content is expressed as

$$LWC = \int_{r_1}^{r_2} \frac{4\pi}{3} r^3 \rho_l n(r) dr \quad (1)$$

where r_i is the radius of particle, r_1 is the smallest droplet size limit, r_2 is the largest droplet size limit, $n(r)$ is the probability density function for the droplet size distribution., and ρ_l is the density of water. The extinction coefficient (Nebuloni, 2005) is calculated as

$$\beta = \int_{r_1}^{r_2} \pi Q_e(r, \lambda) n(r) r^2 dr \quad (2)$$

where Q_e is the extinction efficiency calculated via Mie theory and is a strong function of droplet radius and λ , the wavelength of light. Visibility is related to the extinction coefficient through the equation

$$Vis = \frac{-\ln(\varepsilon)}{\beta} \quad (3)$$

where ε is the contrast limit commonly accepted as 0.02 (Kunkel, 1984).

We see that both liquid water content and visibility are strongly dependent on the size distribution and number concentrations of the droplets formed. For a lognormal droplet size distribution (Podzimek, 1997) the probability density function is,

$$n(r) = \frac{1}{\sqrt{2\pi \ln \bar{\sigma}_g}} \exp \left[\frac{-\left(\ln \frac{r}{\bar{r}_g} \right)^2}{2(\ln \bar{\sigma}_g)^2} \right] \quad (4)$$

where \bar{r}_g is the geometric mean radius and σ is the geometric standard deviation.

Using equations 1-4, visibility was investigated as a function of mean particle radius, LWC , particle concentration, and the geometric

standard deviation of particle size. Results are presented in figures 2 through 6. In Fig. 2-4, the geometric standard deviation of particle size was constant and equal to 1.1 μm . Figure 2 illustrates that as particle mean diameter increases, more LWC is required to achieve the same level of visibility reduction. From Fig. 2, we can find likely particle sizes for desired visibility and a given *LWC* available.

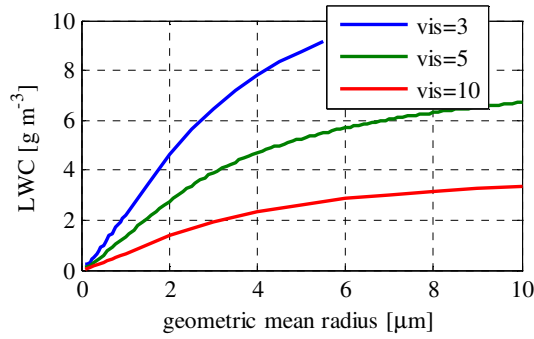


Figure 2: Relationship between *LWC* and geometric mean radius for iso-visibilitys of 3, 5 and 10 meters.

Figure 3 can be used to determine the needed particle concentration given the likely particle size determined from figure 2 and a specified visibility.

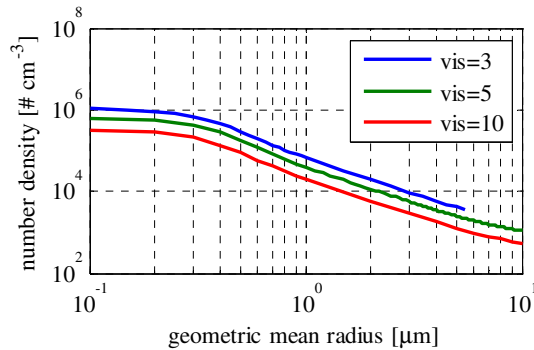


Figure 3: Relationship between number density of droplets and particle radius for iso-visibilitys of 3, 5 and 10 meters.

It is noted that *LWC*, particle concentration and particle size are not independent as shown in figure 4.

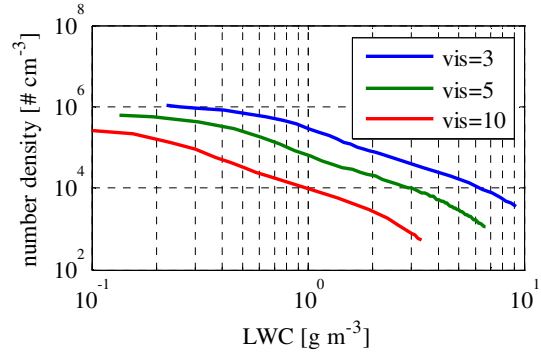


Figure 4: Relationship between number density of droplets and *LWC* for iso-visibilitys of 3, 5, and 10 meters. As expected there lower *LWC* are necessary for defined visibility with greater number concentrations and smaller size droplets.

In Figs. 5-6, the geometric standard deviation of particle size was varied from 1.3 to 2 μm for a fixed visibility of 3 meters. As can be seen in Fig. 5, the effect of standard deviation of the particle size distribution decreases greatly, and particle number converges rapidly, as the mean particle radius increases for a fixed level of visibility. Figure 6 shows influence of particle size spread on required water content.

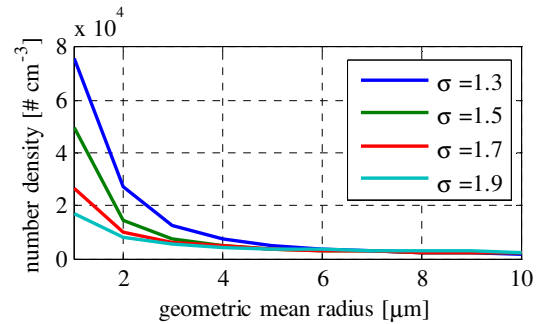


Figure 5: sensitivity study of droplet number concentration to mean geometric radius for visibility set to 3 meters with distribution spread, σ , ranging from 1.3 to 2.

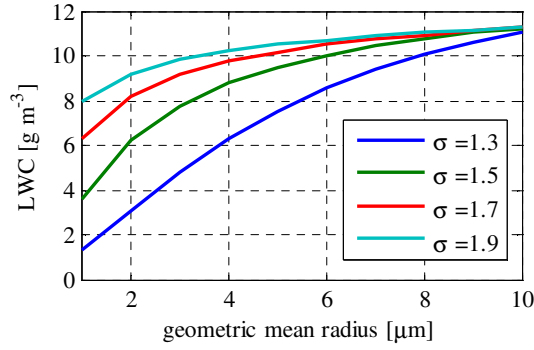


Figure 6: sensitivity study of LWC to mean geometric radius for visibility set to 3 meters with distribution spread, σ , ranging from 1.3 to 2.

Thermodynamic Model

A major factor in superfog formation is the available liquid water. If there is enough moisture available, liquid water results when a warm air mass produced by smoldering mixes with colder ambient air and thermodynamically condenses. The liquid water content strongly depends on the final temperature and saturation vapor pressure of the mixture. A mass balance of water vapor is

$$w_3 = \frac{m_1 w_1 + m_2 w_2}{m_1 + m_2} \quad (5)$$

where w_i is the mixing ratio and m_i is the mass of air ($i=1$ – warm and humid, 2 – cool and dry, 3 – mixture of 1 and 2). An initial estimate of temperature is made through a weighted average.

$$T_3 = \frac{m_1 T_1 + m_2 T_2}{m_1 + m_2} \quad (6)$$

where T_i is the temperature at a states 1, 2 or 3. The final temperature, T_f , is defined as

$$f(T_f) = T_f - T_3 - dT = 0 \quad (7)$$

where dT is temperature changes due to latent energy transfer. A Newton Rapson convergence method was used to iteratively solve for the final mixture temperature (eq. 10).

$$T_f^{i+1} = T_f^i - \frac{f(T_f^i)}{f'(T_f^i)} \quad (8)$$

The excess mixing ratio is expressed a

$$w_l = w_3 - w_s(T_f) \quad (9)$$

where w_l is the excess liquid mixing ratio and $w_s(T_f)$ is the saturation mixing ratio at the final mixture temperature. The excess liquid mixing ratio can be related to the liquid water content by multiplying by the density of air, ρ_a , (eq. 12).

$$LWC = w_l \rho_a \quad (10)$$

Effect of particles on condensation

To this point, the effects of cloud condensation nuclei (CCN) on water condensation have not been considered. In the current formulation, relative humidity will need to exceed 100% for small droplets to form without the presence of particles. However, CCN particles attract water vapor and dissolve to form a droplet solution thus decreasing the saturation vapor pressure as explained by the Kohler equation (Seinfeld and Pandis, 2006):

$$S = \exp\left(\frac{4M_w \sigma_w}{DRT\rho_w} - \frac{6n_s M_s}{D^3 \pi \rho_s}\right) \quad (11)$$

where S is the saturation ratio, M_w is the molecular weight of water, σ_w is the surface tension of water, D is diameter of droplet, R is the ideal gas constant, T is the temperature, ρ_w is the density of water, n_s is the moles of solute per droplet, M_s is the molecular weight of the solute, and ρ_s is the solute density. The saturation ratio is the relative vapor pressure around a sphere compared to the saturation vapor pressure. The

first term in eq. 11 represents the effect due to surface tension that raise the necessary saturation ratio to form droplets, and the second term accounts for the effect due to solutes/particles decreasing the relative humidity necessary to condense.

The Kohler curves for $(\text{NH}_4)_2\text{SO}_4$ (ammonium sulfate) CCN for various concentrations are presented in figure 7. Ammonia groups and other organic compounds are common soluble pollutants associated with biomass burning (Cuss, 2001 ; Mazzoleni et al., 2007). As the amount of solute per droplet increases, so does the ability to attract water vapor to readily condense at a lower relative humidity.

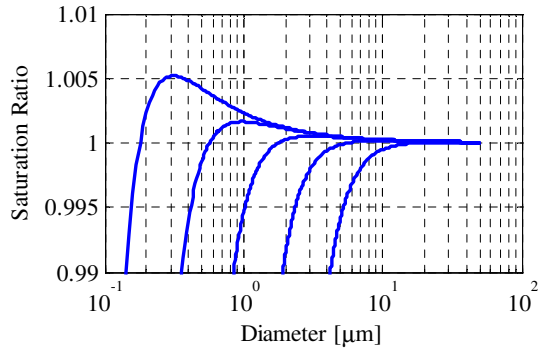


Figure 7: Kohler curves for ammonium sulfate for iso-masses of solute per droplet.

The available pollutant solute concentration, C_s , serve as the CCN. At a specified number density of CCN, the number of moles of solute ions per droplet (n_s) may be represented as

$$n_s = \frac{C_s}{\#CCN} \frac{v}{M_s} \quad (12)$$

where $\#CCN$ is the number density of droplets and v denotes the number of ions that result via disassociation of the solute. Rearranging the Kohler equation, the needed number of moles required to condense water droplets to a specified size is

$$n_s = \left[\frac{4M_w \sigma_w}{DRT\rho_w} - \ln(S) \right] \frac{D^3 \pi \rho_s}{6M_s} \quad (14)$$

Needed and available curves for results of the molar solute concentration at multiple pollution levels are presented in figures 8 and 9.

Table 1. Summary of pollution, LWC and visibility results for 99% RH.

C_s [$\mu\text{g m}^{-3}$]	$D=0.5 \mu\text{m}$		$D=1 \mu\text{m}$	
	LWC [g m^{-3}]	Vis [m]	LWC [g m^{-3}]	Vis [m]
10	0.017	157.0	0.019	530.2
50	0.083	31.3	0.098	106.0
100	0.166	15.6	0.196	53.0
1000	1.662	1.6	1.967	5.3

Table 2. Summary of Laboratory Measurements

Experiment	Warm Air Mass		Cold Air Mass		Mixture		LWC [g kg^{-1}]	Number density	Visibility [m]
	T [$^{\circ}\text{C}$]	RH	T [$^{\circ}\text{C}$]	RH	T [$^{\circ}\text{C}$]	RH			
1	32.2	96.1	8.1	99.1	17.9	>100.0	5.5	49000	3.5
2	27.0	61.8	11.1	98.1	14.9	>100.0	2.0	20000	4.5

Legend for figures 8 and 9:

- needed
- available $C_s=10 \text{ ug m}^{-3}$
- available $C_s=50 \text{ ug m}^{-3}$
- available $C_s=100 \text{ ug m}^{-3}$
- available $C_s=1000 \text{ ug m}^{-3}$

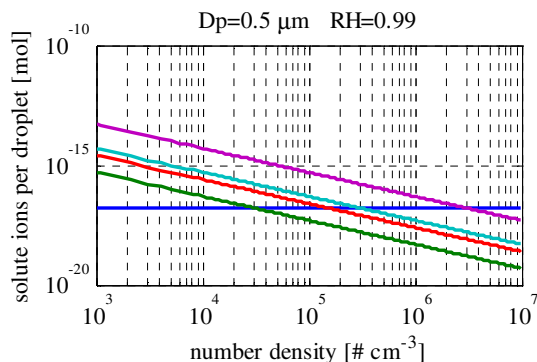


Figure 8: Plot of moles of solute per droplet vs. number density at various air qualities. Droplets were assumed to be $0.5 \mu\text{m}$ in size in an environment of 99% relative humidity. The curves for different concentrations are iso-LWC, however the visibility changes throughout the curves.

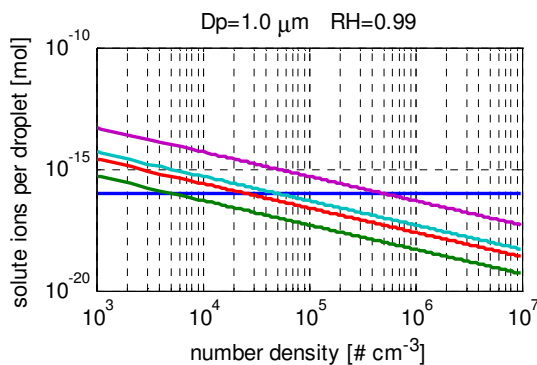


Figure 9: Plot of moles of solute per droplet vs. number density at various air qualities. Droplets were assumed to be $1 \mu\text{m}$ in size in an environment of 99% relative humidity. The curves for different concentrations are iso-LWC, however the visibility changes throughout the curves.

In figures 8 and 9 the needed curve represents the threshold of where condensation may form. The greatest visibility reduction possible for any given solute pollution concentration occurs at the intersection with the needed threshold curve. Table 1 shows the nonlinear relation between the solute concentration, LWC, and visibility. Superfog is achieved if droplets are $0.5 \mu\text{m}$ in size and near-superfog conditions are reached for droplet sizes of $1 \mu\text{m}$.

Laboratory Measurements

A superfog test chamber is designed to simulate the interactions similar to field conditions, through controlled mixing of two air masses with different temperatures and relative humidities. A schematic of the fog chamber is presented in Figure 10. In the experiments, both the cool and warm air masses are pumped through separate ducts into a $300 \text{ cm} \times 200 \text{ cm} \times 200 \text{ cm}$ test chamber for mixing. The test chamber is constructed of transparent acrylic material for visualization. Vane probe anemometers, temperature and relative humidity sensors are placed at the two inlet ducts and on the chamber exhaust.

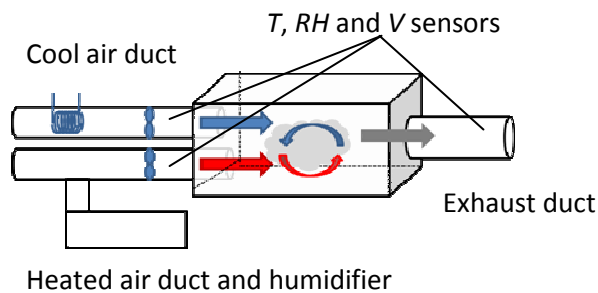


Figure 10: Schematic of fog test chamber

A phase Doppler particle analyzer (PDPA) system was used to measure the size distribution and number concentration of droplets formed through condensation. The fog formed was transported down 1.5 meters of exhaust ducting

to the PDPA for measurements. There were 2 experimental conditions used as outlined in Table 2. Each setup was repeated five times and the results were averaged.

The averages from the conditions and results from the experiments are presented in Table 2. The relative humidity (RH) for position 3, the exhaust, does not present a number because condensation occurred when fog formed, and sensor could not function in conditions over 100% RH. The measured probability density curves for the size distribution are given in figure 11.

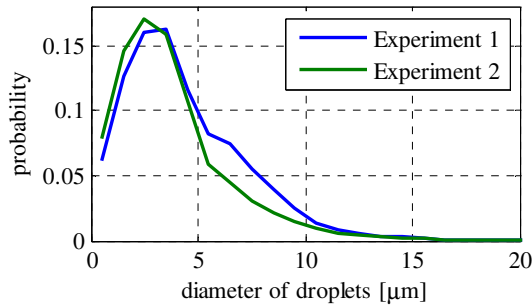


Figure 11: Probability density curve of droplet size distribution measured from the fog test chamber experiments. The green and blue curves represent the averages of experiments 1 and 2.

Discussion

The large liquid water contents ($5 \text{ [g m}^{-3}\text{]}$) to generate superfog conditions are suggested through empirical relations (Kunkel, 1984 and Fisak, 2006). Thermodynamic modeling of various conditions suggested that a LWC of 1 or $2 \text{ [g m}^{-3}\text{]}$ is difficult to achieve. This suggested the importance of available CCNs and their influence on water condensation.

Through the sensitivity studies conducted in this paper it is evident that for droplet distributions with mean size near $1 \mu\text{m}$ or less, and geometric standard deviation near or less than $1.3 \mu\text{m}$, and particle concentrations near 10^5 per cc, it is

indeed possible to have superfog formation at LWC of 1 or $2 \text{ [g m}^{-3}\text{]}$.

Based on the model developed in this paper, we can predict the droplet size distribution that is most likely to result in superfog. It is then logical to investigate the physical processes that lead to such a distribution. From Kohler theory we see that the size of a droplet greatly depends on the concentration, size, and chemical characteristics of the CCN particles.

Regions above the needed threshold curve in figures 8 and 9 represent a range of values for parameters that could result in condensation. The case of droplets being of $0.5\mu\text{m}$ size range in high solute pollution concentration ($1000 \mu\text{g m}^{-3}$) such is the case of a smoldering area, is a situation under which superfog can be readily formed.

Conditions for superfog formation in the laboratory were achieved. Size distribution, number density, LWC and visibilities were recorded for the experiments conducted. The measured of the mean geometric radius ($2.5\text{-}3 \mu\text{m}$) is slightly higher than predictions from modeling ($1\text{-}2 \mu\text{m}$). The experiments and modeling for LWC agree for geometric mean diameter of $2.5 \mu\text{m}$. The number densities for the experiments and the modeling are in agreement. Near superfog conditions were formed for the laboratory experiments.

Nomenclature

LWC	liquid water content
β	extinction coefficient
n_i	number of droplets of index i
r_i	radius of droplet of index i
ρ_l	density of liquid
Q_e	extinction efficiency
Vis	visibility
ε	limit of contrast

r_g	geometric mean radius
σ_g	geometric standard deviation
λ	wavelength of light
w	mixing ratio
T	temperature
S	saturation ratio
M_w	molar mass of water
σ_w	surface tension of water
D	diameter of droplet
R	ideal gas constant
ρ_w	density of water
n_s	moles of solute ions
M_s	molar mass of solute
ρ_s	density of solute
C_s	Concentration of solute pollutant
ν	number of ions per solute molecule when dissociated
Vis	Visibility

Subscripts

1	warm and humid air from smoke
2	cool air from ambient
3	mixture of the 1 and 2 air masses
f	final equilibrium state mixture air mass

Acknowledgements

This work was supported by the USDA/USDI Joint Fire Science Program project 09-1-04-5 administered by USDA Forest Service PSW Research Station agreement 09-JV-11272166-049.

References

[1] Achtemeier, G. (2006). Measurements of moisture in smoldering smoke and implications for fog. *International Journal of Wildland Fire* 15, 517–525

[2] Achtemeier, G. L. (2001). On the Origins of "Superfog" - A Combination of Smoke and Water Vapor that Produces Zero Visibility over Roadways. Second International Wildland Fire Ecology And Fire Management Congress And Fifth Symposium On Fire And Forest Meteorology, November 16-20, Orlando, Florida, p. 1-4

[3] Achtemeier, G. L. (2008). Effects of Moisture Released during Forest Burning on Fog Formation and Implications for Visibility. *Journal of Applied Meteorology and Climatology*, 47(5), 1287.

[4] Achtemeier, G. L. (2009). On the formation and persistence of superfog in woodland smoke. *Meteorological Applications*, 16(2), 215-225.

[5] Achtemeier, G. L., & Service, U. F. (2008). Superfog – Unraveling the Smoke/Fog-on-the-Highway Problem. *Southern Smoke Issues*, Winter 2008.

[6] Asa-Awuku, A. (2008). Investigation of molar volume and surfactant characteristics of water-soluble organic compounds in biomass burning aerosol. *Atmos. Chem. Phys.*, 8, 799-812, 2008.

[7] Chen, Y., & Bond, T. C. (2010). and Physics Light absorption by organic carbon from wood combustion. *Atmospheric Chemistry and Physics*, (2001), 1773-1787.

[9] Collins, J. M., Williams, A. N., Paxton, C. H., Davis, R. J., & Petro, N. M. (2009). Geographical, Meteorological, and climatological conditions surrounding the 2008 interstate 4 disaster in Florida. *Applied Geography*, 153-162.

[9] Dennis, a. (2002). Air pollutant emissions associated with forest, grassland, and

- agricultural burning in Texas. *Atmospheric Environment*, 36(23), 3779-3792.
- [10] Egan. (1974). Measurements of Cloud Condensation Nuclei and Cloud Droplet Size Distributions in the Vicinity of Forest Fires forest fires. *AMS Online Journals*.
- [11] Fišák, J., Řezáčová, D., & Mattanen, J. (2006). Calculated and measured values of liquid water content in clean and polluted environments. *Studia Geophysica et Geodaetica*, 50(1), 121-130.
- [12] Fuzzi, S., Facchini, M. C., Decesari, S., Matta, E., & Mircea, M. (2002). Soluble organic compounds in fog and cloud droplets *Atmospheric Research*, 64, 89 - 98.
- [13] Haefelin, M., Bergot, T., Elias, T., Tardif, R., Carrer, D., Chazette, P., et al. (2010). PARISFOG: Shedding New Light on Fog Physical Processes. *Bulletin of the American Meteorological Society*, 91(6), 767-783.
- [14] Hanna, S. R., Briggs, G. A., & Jr., R. P. (1983). *Handbook on atmospheric diffusion: Atmospheric Environment (1967) (Vol. 17, pp. 673-675).* , Springfield, VA 22161: National Technical Information Service, U.S. Department of Commerce
- [15] Holle, R. (1971). Effects of cloud condensation nuclei due to fires and surface sources during South Florida droughts. *Journal of Applied Meteorology*, 10(1), 62–69.
- [16] Kunkel, B. (1984). Parameterization of droplet terminal velocity and extinction coefficient in fog models. *Journal of Applied Meteorology*, 23(1), 34–41. NOAA Central Library, Department of Commerce.
- [17] Lowe, P. R. (1977). An approximating polynomial for the computation of saturation vapor pressure. *J. Appl. Meteor*, 16(1), 100–103. Retrieved from
- [18] Nebuloni, R. (2005). Empirical relationships between extinction coefficient and visibility in fog. *Applied optics*, 44(18), 3795-3804.
- [19] Ogren, J. a., Heintzenberg, J., Zuber, a., Noone, K. J., & Charlson, R. J. (1989). Measurements of the size-dependence of solute concentrations in cloud droplets. *Tellus B*, 41B(1), 24-31.
- [20] Pagowski, M., Gultepe, I., & King, P. (2004). Analysis and Modeling of an Extremely Dense Fog Event in Southern Ontario. *Journal of Applied Meteorology*, 43(1), 3.
- [21] Parmar, R. S., Welling, M., Andreae, M. O., & Helas, G. (2008). Water vapor release from biomass combustion. *Atmospheric Chemistry and Physics*, (1953), 6147-6153.
- [22] Podzimek, J. (1997). Droplet concentration and size distribution in haze and fog. *Studia Geophysica et Geodaetica*, 41, 277-296.
- [23] Seinfeld, J. H., and Pandis, S. N. (2006), *Atmospheric Chemistry and Physics- From Air Pollution to Climate Change (2nd edition)*, John Wiley & Sons
- [24] Wilck, M. (2001). A general approximation method for solving integrals containing a lognormal weighting function. *Journal of Aerosol Science*, 32(9), 1111-1116.